Theor Chem Acc (2006) 116: 355–372
DOI 10.1007/s00214-005-0011-2

REGULAR ARTICLE

Simon P. Webb

Ab initio electronic structure theory as an aid to understanding excited state hydrogen transfer in moderate to large systems

Received: 27 April 2005 / Accepted: 11 August 2005 / Published online: 24 November 2005

Abstract Hypocrellin and hypericin are naturally occurring polycyclic perylene quinones, and they have both been found to exhibit photoactivated antiviral and anticancer activity. One mode of action proposed involves excited state hydrogen transfer. Consequently, these compounds have been widely studied using spectroscopic methods, and are found to both absorb and emit in the visible region. Recently, an analog dihydroxy perylene quinone was synthesized in order to examine its antiviral activity in relation to the naturally occurring compounds. Its UV-visible absorption and emission spectra are quite different to those of hypocrellin and hypericin, with very weak absorption and no emission at all in the visible region. The ab inito excited state methods, configuration interaction singles (CIS), state-averaged complete active space self-consistent field, and state-averaged-multireference perturbation theory are used to examine the origin of this different absorption and emission behavior. Due to the size of these systems (between 24 and 40 heavy atoms) extensive use of parallel processor algorithms was made, especially a parallel atomic orbital-based CIS energy and gradient code developed at the ABCC. The performance of these methods and possible future directions are discussed.

Keywords Hypocrellin · Hypericin · Perylene quinones · Excited states · Hydrogen transfer · Parallel processor CIS · CASSCF · MRMP2

1 Introduction

Electronic structure theory methods are now used routinely for the determination of ground state potential energy surfaces and properties. Conversely, the computational study of excited state chemical reactions is far from routine. This article will examine the use of theoretical chemistry as an aid to understanding the excited state chemistry of moderate to large chemical systems (large for ab initio calculations); with particular emphasis on excited state intra-molecular hydrogen transfer reactions and interpretation of UV-visible spectra. Our approach is to apply ab initio excited state theoretical chemistry methods to a number of systems in which excited state hydrogen transfer can occur, make comparisons to available experimental data, and then assess the performance of the methods with a view to ongoing and future methodological developments as well as future application studies.

Hypocrellin and hypericin (see Figs. 1a, b) are naturally occurring polycyclic perylene quinones, and both exhibit photoactivated antiviral [1,2] and anticancer activity [3–5]. A number of mechanisms of action have been proposed: one involves formation of singlet oxygen via energy transfer from a quinone triplet state; another requires interaction of the excited quinone with molecular oxygen followed by electron transfer leading to the formation of a radical superoxide anion and a radical quinone cation [6,7]. Petrich and co-workers propose yet another mechanism in which excited state hydrogen/proton transfer plays a role in biological activity [8–10], and have carried out a series of spectroscopic studies aimed at elucidating the fundamental photophysical behavior of hypocrellin, hypericin, and related compounds [11–14]. Our ultimate goal is to use theoretical chemistry methods to compliment these experimental studies and help further the understanding of the excited state behavior of this class of compounds in general.

This goal is a considerable challenge to theoretical chemistry. First, the size of these systems (∼40 heavy atoms) is large, especially for the application of high level excited state ab initio methods. Also, excited state processes often involve conical intersections [15–17] or the close approach of potential energy surfaces leading to nonadiabatic effects such as vibronic coupling [18]. Another issue in these particular systems is solvation; while the excited state hydrogen transfer rate in hypericin does not exhibit a solvent dependence [19], in hypocrellin there is a dependency on solvent viscosity [20, 21]. To add a further complication, hydrogen quantum tunneling effects have been proposed in explanations of some of the hypocrellin/hypericin spectroscopic data [11,14,22,23].

S.P. Webb
Advanced Biomedical Computing Center,
SAIC-Frederick, Inc., National Cancer Institute at Frederick,
P.O. Box B, Frederick, MD 21701, USA

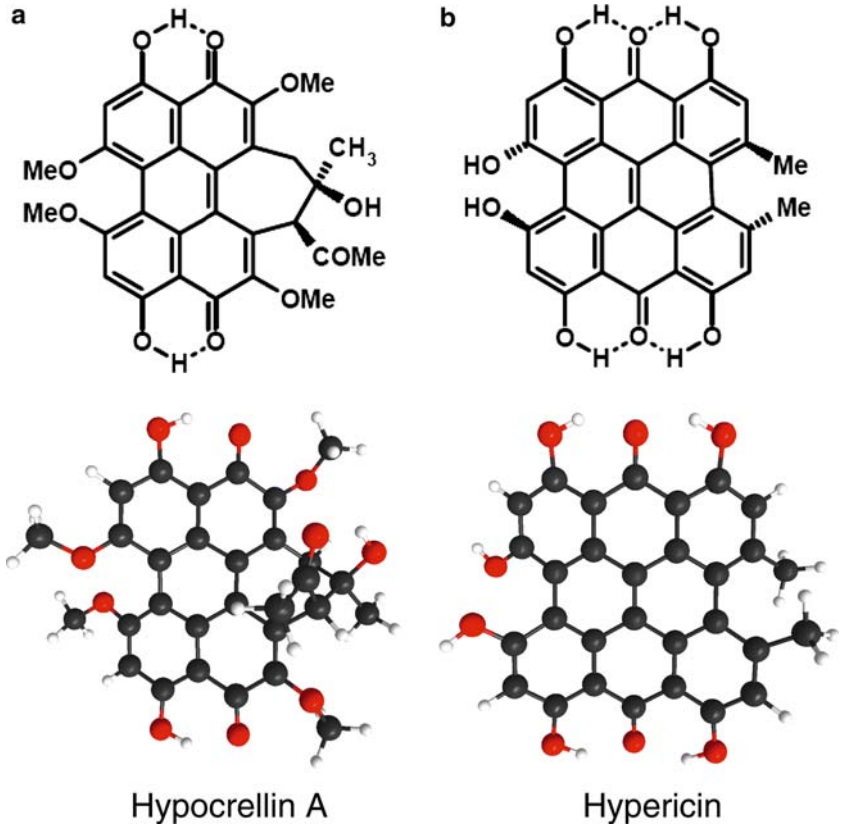

Fig. 1 Structures of hypocrellin A and hypericin

In order to place our particular computational approach to these systems in context, as well as provide background for the discussion of future directions, there now follows a brief outline of some of the currently available theoretical chemistry methods for dealing with excited state processes and the issues just described.

Excited state electronic structure methods are considerably more complicated and are typically more expensive, in terms of computer resources, than their ground state counterparts. The most straightforward excited state method is configuration interaction with single substitutions (CIS) [24]. It is also the least demanding computationally, and as Foresman et al. [24] pointed out in 1992, it can be formulated in an algorithm based on the construction of Fock-like matrices, which circumvents the need for integral transformations from the atomic orbital (AO) to the molecular orbital (MO) basis. CIS analytic gradients have been derived [24,25], facilitating the determination of excited state stationary points, numerical Hessians, and minimum energy paths (MEPs). Analytic CIS Hessians have also been derived and implemented [26]. Efficient CIS energy and gradient parallel processor algorithms have been developed [27] and CIS calculations run on parallel processors can be routinely applied to systems of a thousand basis functions or more (see computational methods section).

CIS is considered to be the excited state equivalent to ground state Hartree-Fock (HF) methods, and CIS relative energies of excited state stationary points are comparable to ground state HF relative energies in quality. CIS, like HF, does not include the effects of dynamic electron correlation. As a consequence, vertical transition energies obtained from CIS are consistently too large, especially when double-excitations are important. Attempts have been made to simply scale CIS transition energies, and in this case oscillator strengths (OS) can be used to match calculated vertical absorptions with intense spectral peaks. More sophisticated approaches include an ad hoc perturbation treatment (CIS(D)) [24,28], which has recently been found to provide quite consistent agreement with lower energy peaks in absorption spectra [29]. The addition of selected double excitations results in considerable improvement for transitions from open shell reference ground states [30,31] which are quite poor otherwise. Another approach by Grimme [32] has been to adjust the two-electron terms in the CIS energy expression using fitted coefficients in a mixed density functional theory/CIS (DFT/CIS) approach. Clearly, CIS should be used with its shortcomings in mind; however, the method remains useful for determination of the qualitative nature of transitions [33] and the determination of excited state geometries of large systems. Of course, CIS cannot be used even in a qualitative sense if the ground state itself is multiconfigurational in character.

Among the most complex excited state techniques are multiconfigurational self-consistent field (MCSCF) based methods [34]. Complete active space self-consistent field

(CASSCF) [35], also referred to as fully optimized reaction space MCSCF (FORS-MCSCF) [36], includes all electronic excitations within a given active space and also optimizes the MOs to self consistency. An advantage of CASSCF is that it can qualitatively describe complex radical ground state and excited state systems involving near orbital degeneracy (HOMO-LUMO degeneracy for the ground state) [34]. For example, radical systems, like those formed in homolytic bond breaking/making processes or in unsaturated low-spin metal systems [37,38]. The CASSCF method requires that an active space be chosen that is suitable for the chemistry under study. A number of approaches can be taken to generate active spaces. HF canonical orbitals may be modified to make the choice of chemically relevant orbitals more obvious. For occupied orbitals, orbital localization schemes [39] are often used (retaining any symmetry present); other schemes exist for virtual orbitals [40]. Another choice is to carry out a limited CI (e.g. singles and doubles) in an extended space to generate natural orbitals, which can be sorted according to the level of mixing by their occupation numbers. In any case, it is important to examine closely the active orbitals in any MCSCF approach. In addition, convergence with respect to the number of active space orbitals should be considered.

The full configuration interaction (FCI) step in CASSCF rapidly becomes intractable. This is also true of the required AO to MO transformation with increasing size of the active space and AO basis set. Modern implementations of CASSCF employ direct FCI methods [41] and currently millions of configurations can be handled on a routine basis. Parallel processor CASSCF algorithms also exist, which scale reasonably well, removing the AO to MO transformation bottleneck allowing for quite large basis set cases. Parallelization of the FCI step has also been addressed [42,43]. Even so, in order to circumvent to some degree the rapid increase of the number of configurations in the FCI step, occupation restrictive CI methods have been developed. For example, restricted active space SCF (RASSCF), allows three spaces, and the user defines the allowed excitations (subject to certain criteria) within and between spaces [44–47]. More recently, CI methods that allow a completely arbitrary choice of spaces and occupations have been developed [48–50]. The ab initio direct determinant occupation restricted multiple active spaces (ORMAS) method has also been integrated with orbital optimization techniques (ORMAS-SCF) [48,49].

CASSCF and similar approaches do not account for dynamic electron correlation effects. In the case of excitation energies, while CASSCF will usually correctly describe the qualitative nature of transitions, it will not in general give quantitatively accurate transition energies. For more quantitative accuracy, the CASSCF wavefunction can be used as a reference for a subsequent perturbative treatment to account for dynamic correlation. Complete active space second order perturbation theory (CASPT2) due to the Roos group was the first of these methods [51,52]. Other similar approaches have been developed [53,54], as well as a multistate version: multiconfigurational quasidegenerate perturbation theory (MCQDPT) [55,56]. Another quasidegenerate method is generalized Van Vleck perturbation theory (GVVPT2) due to Hoffmann [57]. These multireference perturbation theory methods have been able to accurately predict vertical transition energies to multiple states for many systems [58,59]. They are, however, quite expensive in terms of computational resources, which can limit their applicability.

Time dependent density functional theory (TDDFT) [60, 61], like its ground state counter part, includes some dynamic electron correlation effects and generally offers improved results for transition energies over CIS. For low lying valence excited states its accuracy can be similar to that of the more expensive multiconfigurational reference perturbation methods described above. The method is now widely used; however, it does have limitations in its present form, for example, it has problems with long-range charge-transfer systems [62–64]. In addition, TDDFT, like CIS, is an inherently single-determinant reference single excitation method, and as such it is not well suited for systems where double excitations are important [65] or that have large multiconfigurational ground state character [66]. One promising attempt to solve this problem is the development of DFT/MRCI [67, 68]; a recent MCSCF-DFT development is of interest also [69]. Efficient parallelized TDDFT algorithms are available allowing calculation of vertical excitation energies for large systems [70]. Analytic gradients have only recently become available [71–74], and studies using TDDFT to examine excited state surfaces [75,76] have begun to appear in the literature.

It should be noted that extremely accurate approaches to the calculation of excited state energies include multireference CI (MR-CI)[41], multireference coupled cluster methods (MR-CC), for example [77–79], and equation of motion coupled cluster (e.g. EOM-CC variants), for example [80–83]. These methods are currently prohibitively expensive for more than four or five heavy atoms, but their extremely high degree of accuracy makes them very useful for understanding small systems in great detail and in the benchmarking of other methods, which can be used with larger systems. Also, more economical EOM methods, which provide good quality results, are now available. Similarity transformed EOM coupled cluster theory (STEOM-CC) is quite accurate for systems dominated by single excitations (it can also be more cheaply applied to perturbation theory (STEOM-PT)) [84,85]. Extended-STEOM-CC [86] provides more accurate excitation energies when double excitations are important. A localized orbital EOM-CCSD method [87] allows for much larger systems to be examined with little loss in accuracy. However, we note that despite the reduced cost of these latter methods, they are still presently too costly to apply to the $\sim$40 heavy atom systems we are considering.

Solvation can have a large effect on excited state chemistry. Obvious examples are solvent shifts in UV-visible spectroscopy. Ground state electronic structure theory solvation methods are now quite well established. These include continuum methods [88], for example, the polarizable continuum model (PCM) [89]. An alternative type of approach is the inclusion of explicit solvent via quantum mechanics molec-

ular mechanics (QM-MM) approaches [90]. One example is the effective fragment potential (EFP) method [91,92], which treats the solvent with a highly sophisticated potential that includes electrostatic, polarization, and exchange repulsion terms. The EFP method has been shown to be capable of reproducing full ab initio solvation results and has provided valuable insights into solvation effects for a wide range of solutes [93–99]. The extension of these implicit and explicit solvation models to excited states is well under way. Karelson and Zerner [100] discussed the use of the self-consistent reaction field method with the intermediate neglect of differential overlap (INDO) semiempirical excited state method in 1992. Since this time extension of the PCM method for use with various excited state methods has occurred, including CIS [101], CI and CASSCF [102], and TDDFT [103]. Explicit solvent QM-MM methods have also been extended to allow for excited states: CASSCF-EFP excited state calculations were first carried out some time ago [104]. Recently, a TDDFT-MM method has become available [105]. Indeed, this is currently a very active area of research.

Often in excited state reactions or photophysical processes, electronic surfaces cross (conical intersections) or approach closely leading to vibronic coupling effects, and this can have a large effect on spectra. Ideally, one would calculate derivative nonadiabatic coupling matrix elements between the various electronic-vibrational states. These derivatives can be calculated analytically at the ab initio level for very small systems [18,106]. Quite recently, methodology has been developed for first-principles simulations of UV-visible absorption spectra [107,108]. In this particular approach numerical differentiation of diabatic potential energy matrix elements, obtained from a unitary transformation of the adiabatic vertical excitation energies, is carried out. This approach is presently limited to quite small systems as many energy calculations at high levels of theory are required.

The light mass of the hydrogen nucleus results in significant quantum effects in hydrogen transfer reactions. The electronic ground state dynamical effects of hydrogen tunneling have been investigated extensively by a number of groups, for example, Hynes and co-workers [109], and Truhlar and co-workers [110,111]. Another example is Hammes-Schiffer and co-workers, who have developed a mixed quantum classical approach called molecular dynamics with quantum transitions (MDQT) [112]. In this approach only the transferring hydrogen is treated quantum mechanically and the rest of the system is treated with molecular mechanics, so it can be applied to very large systems such as enzymes [113,114]. Ground and excited state hydrogen vibrational wavefunctions are calculated at each time step numerically on a grid using, for example, the Fourier grid Hamiltonian MCSCF (FGH-MCSCF) [115,116] method. Our present goals, however, require electronic excited states and electronic structure methods. Martinez and co-workers have developed a semiemperical electronic structure based dynamics method, ab initio multiple spawning (AIMS) [117]. While this method was initially designed to account for nuclear quantum effects associated with nonadiabatic transitions, it has now been extended to incorporate tunneling effects [118]. In static electronic ground state ab initio electronic structure calculations, the nature of hydrogen quantum effects has been examined by construction of hydrogen potentials along MEPs or straight-line paths, and numerical calculation of the hydrogen nuclear wavefunction [119]. This approach, in principle, can also be applied to electronic excited states. For a relatively small system, Guallar et al. [120] constructed an excited state keto-enolic tautomerization PES at the CIS level of theory and carried out semiclassical dynamics of intramolecular proton transfer. Recently, attempts have been made to include nuclear quantum effects directly in ab initio calculations of hydrogen transfer, resulting in the nuclear-electronic orbital (NEO) methods (NEO-CI, NEO-MCSCF) [121]. Application to hydrogen transfer has proved to be very challenging due to large nuclear-electron correlation effects [122]. Considerable progress continues to be made though [123,124].

As alluded to earlier, a complete computational description of the excited state behavior, including excited state hydrogen transfer, of the naturally occurring perylene quinones (Fig. 1), would require inclusion of nonadiabatic effects, solvation effects, and hydrogen tunneling effects (ideally all included in dynamic simulations). We have just seen above that sophisticated methodology exists that is designed to account for just these types of effects. However, due to the cost of ab initio potentials, we are presently limited to a straightforward Frank-Condon adiabatic approach: absorption transition energies calculated at ground state geometries; emission transition energies calculated at the excited state geometries, and any nonadiabatic effects, for example vibronic coupling, must be inferred from the close approach of adiabatic surfaces. In addition, solvation and tunneling effects will be addressed in the future depending on the findings of this study. Even so, the required calculation of excited state minima, transition states, and in some cases MEPs, as well as vertical absorption energies, is a far from trivial task for these systems. Our initial goal, then, is to establish levels of theory able to aid in the interpretation of the gross features of steady state UV-visible spectra obtained for the naturally occurring perylene quinones, and related compounds (Figs. 1, 2, 3, 4), and we present our initial steps towards this here.

A brief outline is as follows. The first systems we consider are from a previous collaboration with Petrich and co-workers [125], and are synthetic analogs of hypocrellin/hypericin, containing a simple perylene core (these are referred to throughout as *analogs*). The dihydroxy system (see Fig. 2a, b) offers the possibility of hydrogen transfer, while the methoxy system (see Fig. 2c, d) does not. UV-visible spectra are available for comparison (see Fig. 4), and the smaller size of the systems (24 and 26 heavy atoms) allows high levels of theory to be explored more easily. Having established levels of theory that appear to reproduce and interpret important features of the spectra, these same levels of theory are then applied to a model system, 4,9-dihydroxyperylene-3,10-quinone, (24 heavy atoms – see Fig. 2e, f, these are referred to throughout as *model system*), which more closely resembles hypocrellin. As no experimental data exists for this molecule,

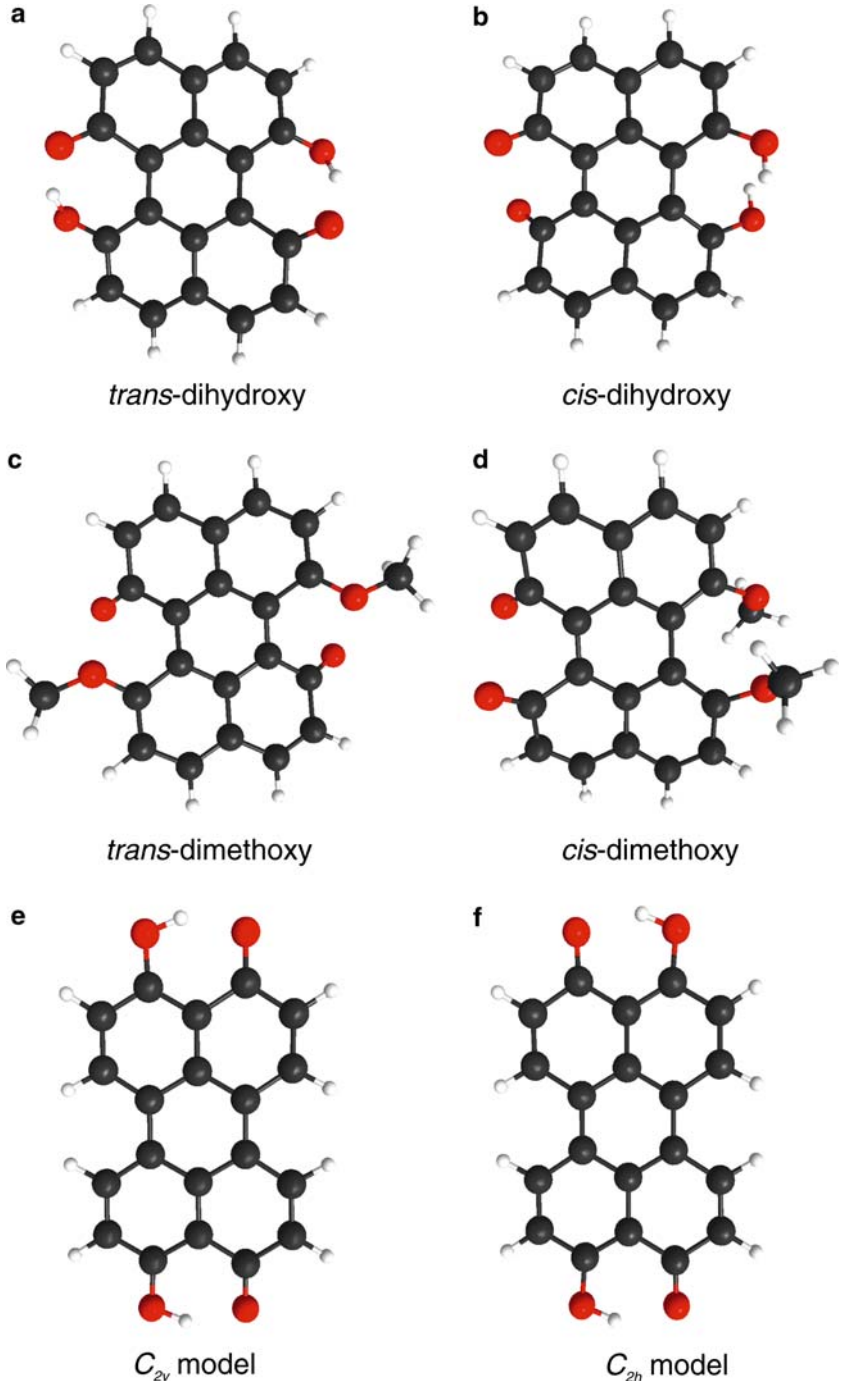

Fig. 2 Structures of the analog compounds **a** C_2 *trans*-dihydroxy, **b** C_2 *cis*-dihydroxy, **c** C_2 *trans*-dimethoxy, and **d** C_2 *cis*-dimethoxy perylene quinone, and the hypocrellin **e** C_{2v} model system, and **f** C_{2h} model system

the purpose of these calculations is to compare and contrast with the previous analog systems and spectra, as well as with any subsequent calculations on the actual hypocrellin/hypericin systems and their spectra. We then present initial results for the hypocrellin A molecule and discuss them in the context of the analog and model system results. An assessment of the results and future directions and developments follow.

2 Computational methods

All ground state singlet (S_0) structures were determined using the Restricted Hartree-Fock (RHF) method. Stationary points (zero gradient structures) were characterized by calculation and diagonalization of the Hessian (matrix of the energy second derivative): all positive eigenvalues indicate a minimum

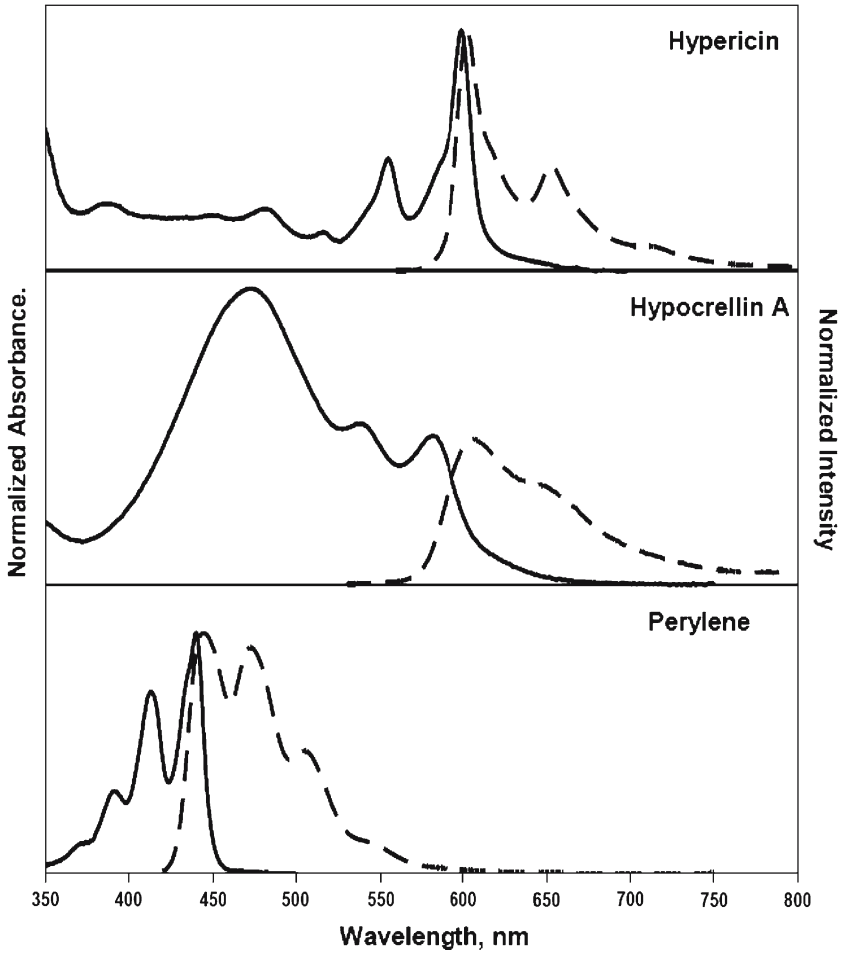

Fig. 3 Absorption (*solid line*) and fluorescence spectra (*dashed line*) of hypericin, hypocrellin A, and perylene (for comparison) in DMSO

on the potential energy surface, and one negative eigenvalue indicates a transition state. For the analog and model compounds (Fig. 2a–f), MEPs were calculated, using the intrinsic reaction coordinate method of Gonzales and Schlegel [126], with a step size of 0.3 $amu^{1/2}$ -bohr, to confirm that minima were correctly associated with transition states. Pople's double-ζ split-valence basis set with polarization functions on heavy atoms [127–129], i.e., 6-31G(d), was used for the determination of all geometries and MEPs. Ground state relative energies including the effects of dynamic electron correlation were determined through second-order perturbation theory [130] (MP2/6-31G(d)//RHF/6-31G(d), where "Method A//Method B" denotes a single-point energy calculated using Method A at an optimized geometry determined using method B). All relative energies reported are at 0 K, with no zero point energy corrections.

For all cases, initial vertical excitation energies, $S_0 \rightarrow S_{1-5}$, were calculated via singlet excited state single-point energies at ground state geometries, using the configuration interaction with single excitations (CIS) [24] method (CIS/6-31G(d)//RHF/6-31G(d) energies). CIS/6-31G(d) OS were also calculated. Singlet excited state relaxed geometries were determined using the CIS/6-31G(d) level of theory for all systems.

Subsequently, for the analog and model systems, CASSCF [35,36] calculations with the 6-31G(d) basis set (CASSCF/6-31G(d)//RHF/6-31G(d) energies) and a polarized triple-ζ split-valence basis set [131] (CASSCF/6-311G(d,p)//RHF/6-31G(d) energies) were carried out. Finally, multireference perturbation theory to second-order (MRMP2) calculations (energies were taken from the MCQDPT [55,56] effective Hamiltonian diagonal elements) with the 6-31G(d) and 6-311G(d,p) basis sets (MRMP2/6-31G(d)//RHF/6-31G(d) and MRMP2/6-311G(d,p)//RHF/6-31G(d) energies) were carried out to account for dynamic electron correlation. Vertical excited singlet state to ground state transition energies $S'_n \rightarrow S'_0$ were also calculated using CASSCF and MRMP2 (where the prime indicates the calculation was carried out at the CIS/6-31G(d) excited state geometry).

An eight-electron, eight-orbital (8e,8o) active-space was employed in all CASSCF and MRMP2 calculations, and all valence electrons were included in the MRMP2 perturbation treatment. An initial indication of the required size of the active space was gained from the CIS natural orbital occu-

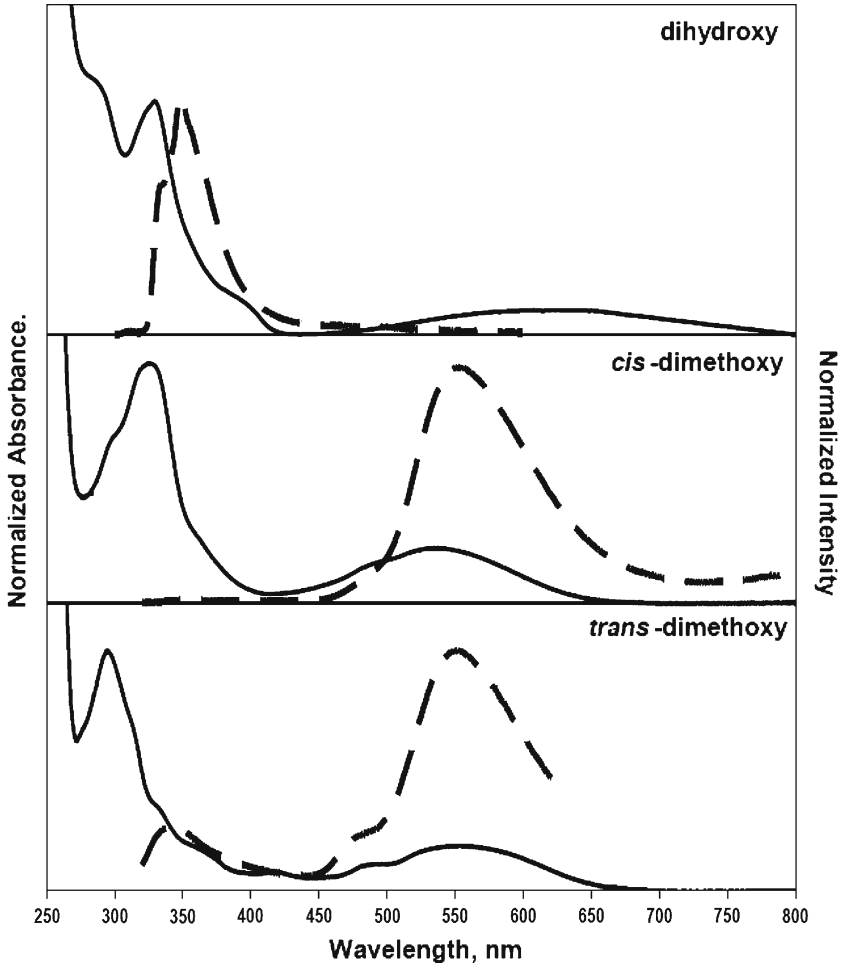

Fig. 4 Absorption (*solid line*) and fluorescence spectra (*dashed line*) of the dihydroxy and the *cis* and *trans* dimethoxy quinones in DMSO

pation numbers for the states considered. The actual $\pi\pi^*$ active space initial guess orbitals were generated using the modified virtual orbital (MVO) procedure due to Bauschlicher [40]. To further check the adequacy of the eight electron, eight orbital active space, as well as to insure that the most suitable orbitals are contained in this smaller space, twelve-electron twelve orbital CASSCF calculations were carried out (to convergence in most cases) and the resulting natural orbitals used as an initial guess for the smaller CASSCF MRMP2 reference. Inspection of the converged canonical $\pi\pi^*$ active space orbitals revealed that they reside mainly in the aromatic core; however, several of the orbitals have some small amount of oxygen *p*-character also. We note that two types of CASSCF and MRMP2 calculations are presented. In one type, denoted symmetry state averaged CASSCF and MRMP2 (SSA-CASSCF and SSA-MRMP2), state averaging was performed only over states of the same symmetry. For example, for C_2 point-group symmetry, a calculation for each irrep is required: one averaged over the first three ^1A states; another averaged over the first three ^1B states. In the other type, simply denoted state averaged CASSCF and MRMP2 (SA-CASSCF and SA-MRMP2), no symmetry was imposed and averaging over the first six states was performed.

All calculations were carried out using the electronic structure theory software package GAMESS [132]. We made extensive use of our frozen-core CIS energy and analytic gradient program, which we implemented in the GAMESS package some time ago. This efficient AO based CIS algorithm, which relies on a series of Fock-like matrix builds, can either be run fully direct with no disk storage of AO integrals or CIS Hamiltonian matrix elements, or alternatively only AO integrals can be stored. It has very moderate memory demands and is very suited to parallel processing, scaling with the number of processors similarly to the HF ground state methods. Figure 5 shows the wall clock scaling for one to 64 processors for three systems: a moderately sized system (*trans*-dihydroxy perylene quinone (Fig. 2a), 6-31G(d)), comprising 380 basis functions, a larger system comprising 652 basis functions (hypocrellin A (Fig. 1a), 6-31G(d)), and a larger system still, comprising 990 basis functions (*trans*-dihydroxy perylene quinone (Fig. 2a), cc-pVTZ [133]). All calculations were carried out on an IBM p595 (64 SMP Power 5 PC 1900 MHz),

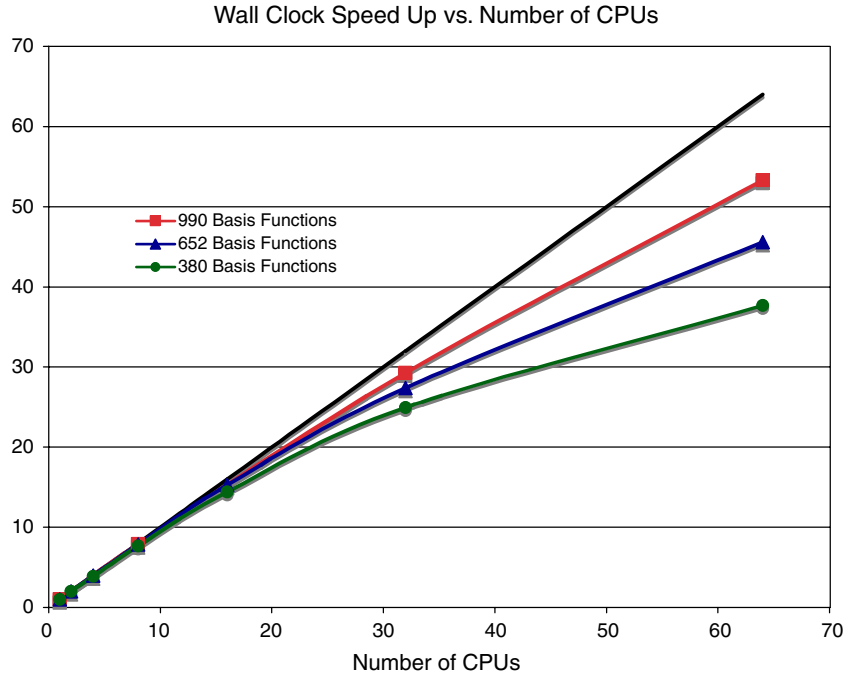

Fig. 5 Speed up curves for CIS parallel energy (five excited states) plus gradient calculation (See Table 1 for details)

Table 1 Wall clock and CPU timings in seconds for the CIS energy and gradient parallel processor algorithm (speed ups are in brackets). All calculations were run fully direct on a 64 SMP Power PC 5 (1900 MHz) IBM P595. Five excited states plus the gradient of the first excited state were calculated. Timings include RHF SCF step starting from an initial Huckel guess

	380 basis functions[a]		652 basis functions[b]		990 basis functions[c]	
CPUs	Wall clock	CPU[d]	Wall clock	CPU[d]	Wall clock	CPU[d]
1	5238	5236	30457	30433	298020	297774
2	2627 (1.99)	2623 (2.00)	15257 (2.00)	15238 (2.00)	–	–
4	1345 (3.89)	1332 (3.93)	7675 (3.97)	7642 (3.98)	–	–
8	685 (7.65)	669 (7.83)	3882 (7.85)	3845 (7.91)	37836 (7.88)	37677 (7.90)
16	363 (14.43)	343 (15.28)	1996 (15.26)	1955 (15.57)	–	–
32	210 (24.94)	181 (28.87)	1112 (27.39)	1017 (29.92)	10190 (29.25)	9915 (30.03)
64	139 (37.68)	104 (50.36)	668 (45.59)	538 (56.51)	5593 (53.28)	5082 (58.60)

[a] Dihydroxy 6-31G(d) system (Fig. 2a) with 81 occupied MOs, 24 of these frozen-core, resulting in 17043 CIS configurations
[b] Hypocrellin A 6-31G(d) (Fig. 1a) with 143 occupied MOs, 40 of these frozen-core, resulting in 52427 CIS configurations
[c] Dihydroxy system cc-pVTZ (Fig. 2a) with 81 occupied MOs, 24 of these frozen-core, resulting in 51813 CIS configurations
[d] Total CPU time averaged over the number of CPUs

requesting the CIS energies of the first five excited states and the gradient of the lowest energy excited state. Table 1 shows the wall clock and CPU timings in seconds. Inspection of Table 1 and Fig. 5 shows that for the 380 and 652 basis function systems on 16 CPUs good speed up (14.4 and 15.3, respectively) is obtained, but there is some reduction in returns on going to 32 CPUs (24.9 and 27.4, respectively). It should be noted that, as expected, better speed up performance is seen with increasing system size, with impressive wall clock speed ups of 29.3 and 53.3 for the 990 basis function case, for 32 and 64 CPUs respectively. CPU timings (which are averages of the total CPU time over the number of CPUs) are informative. Clearly, on reaching 32 CPUs there are some issues regarding CPU utilization. The algorithm is designed to keep communications to a minimum and inspection of timings for each individual CPU in the 32 and 64 CPU runs reveals that load balancing, not data communication, is probably a large part of this problem. In conclusion, our CIS parallel algorithm exhibits very good speed up and enables the routine calculation of CIS transition energies, geometries, and frequencies for systems that on a single CPU would not be practical.

3 Results and discussion

3.1 Dihydroxy and dimethoxy perylene quinones (analog systems)

Figure 2a–d shows the dihydroxy and dimethoxy perylene quinone synthetic analog systems, and Fig. 4 shows their corresponding steady state UV-visible spectra. These systems,

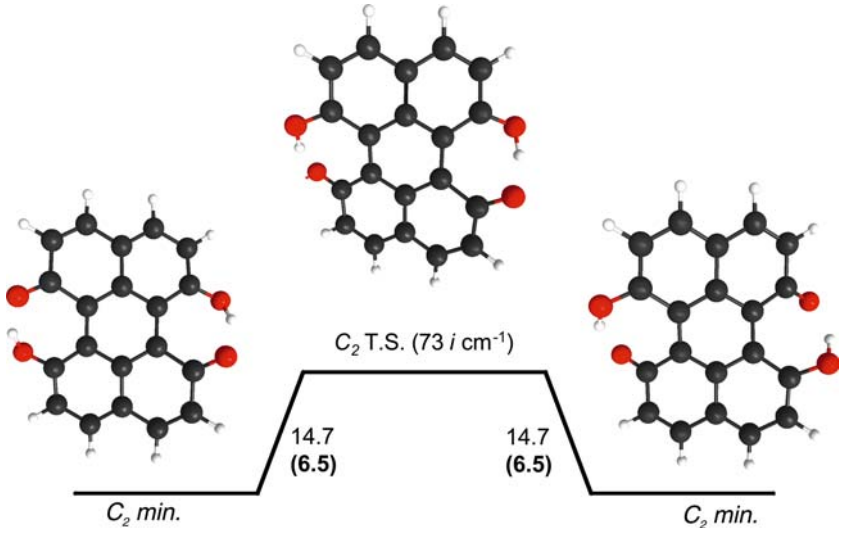

Fig. 6 Ground state double hydrogen transfer in the *trans*-dihydroxy perylene quinone (Fig. 2a). RHF/6-31G(d) energy barrier and MP2/6-31G(d)//RHF/6-31G(d) energy barrier (*bold* and in *brackets*) are given in kcal/mol (0 K and no ZPE). RHF/6-31G(d) imaginary frequency also given

Table 2 Vertical absorption energies, calculated at various levels of theory, in nm and kcal/mol (brackets) for C_2 *trans*-dihydroxy perylene quinone (Fig. 2a)

	$S_0 \rightarrow S_1$	OS	$S_0 \rightarrow S_2$	OS	$S_0 \rightarrow S_3$	OS	$S_0 \rightarrow S_4$	OS	$S_0 \rightarrow S_5$	OS
CIS[a]	^1B 365 (78.3)	0.424	^1A 342 (83.7)	0.012	^1B 298 (96.1)	0.077	^1A 258 (110.4)	0.000	^1B 256 (111.7)	0.126
SSA-CASSCF[b]	^1B 331 (86.4)	0.263	^1A 319 (89.7)	0.002	^1B 318 (90.0)	0.075	^1A 249 (114.9)	0.000	^1B 231 (123.9)	0.159
SSA-MRMP2[c]	^1A 555 (51.5)	0.002	^1B 533 (53.7)	0.075	^1B 480 (59.5)	0.263	^1A 355 (80.6)	0.000	^1B 323 (88.5)	0.159

[a]CIS/6-31G(d)//RHF/6-31G(d)
[b]SSA-CASSCF(8e,8o)/6-311G(d,p)//RHF/6-31G(d), averaging is over three states of each symmetry
[c]SSA-MRMP2(8e,8o))/6-311G(d,p)//RHF/6-31G(d), averaging is over three states of each symmetry

their steady state UV-visible absorption and emission spectra, and ab initio calculations of their transition energies have been discussed in a recent study by Petrich, Webb, Gordon, and additional collaborators [125]. The study was initiated to examine simple analogs of the natural perylene quinones, containing the perylene core, in regards to their UV-visible spectra and antiviral activity. We will summarize our previous results here, but refer the reader to the original paper for a more detailed account.

The initial interpretation of the dihydroxy UV-visible spectrum (Fig. 4) was that the narrow blue band at ∼350 nm and the broader lower intensity band at ∼450–800 nm suggested two forms: a *trans* isomer and a *cis* isomer (Fig. 2a, b), which could tautomerize freely between each other. This also appeared to explain the observation of only two kinds of aromatic ring proton in the NMR spectrum. However, when the dimethoxy compounds were synthesized and their UV-spectra measured, an intense narrow band in the UV and a weak broad band in the visible were seen for *both* the *cis*- and *trans*-dimethoxy species. As no tautomerization can possibly occur between these species, the original explanation of the dihydroxy spectrum was clearly incorrect.

Ground state MP2 calculations showed that the lowest energy *cis*-dihydroxy isomer was 12.5 kcal/mol higher in energy than the lowest energy *trans* isomer, suggesting that only the *trans* isomer is present. Furthermore, the ground state barrier to a double hydrogen transfer in the *trans*-dihydoxy isomer, depicted in Figure 6, leading to an equivalent degenerate minimum, was found to be only 6.5 kcal/mol. Such a hydrogen transfer process, if fast enough, also explains why NMR only detected two types of aromatic ring protons. Calculated emission transition energies also suggest that only the *trans*-dihydroxy isomer is present (see below).

To demonstrate the effects of level of theory, Table 2 shows CIS, SSA-CASSCF, and SSA-MRMP2 vertical transition absorption energies for the *trans*-dihydoxy isomer (at the RHF/6-31G(d) ground state C_2 geometry). As expected, CIS and SSA-CASSCF overestimate the transition energies compared to the SSA-MRMP2 results, indicating the importance of dynamic electron correlation effects. A change in the ordering of the states between both CIS and SSA-CASSCF and the dynamically correlated SSA-MRMP2 can be seen, with a ^1A state becoming the first excited state at the SSA-MRMP2 level of theory (this is a general finding for these analog systems). The SSA-MRMP2 transition energies appear to match the gross features of experimental absorption spectrum (Fig. 4) quite well. We now examine the SSA-MRMP2 vertical absorption and emission transition energies, along with SSA-CASSCF OS, for all the analog systems (Tables 3, 4, Fig. 2a–d).

Table 3 SSA-MRMP2(8e,8o)/6-311G(d,p)//RHF/6-31G(d) absorptions in nm and kcal/mol (in brackets)

Compound	$S_0 \rightarrow S_1$	OS	$S_0 \rightarrow S_2$	OS	$S_0 \rightarrow S_3$	OS	$S_0 \rightarrow S_4$	OS	$S_0 \rightarrow S_5$	OS
trans-dihydroxy (C_2)	^1A 555 (51.5)	0.002	^1B 533 (53.7)	0.075	^1B 480(59.5)	0.263	^1A 355 (80.6)	0.000	^1B 323 (88.5)	0.159
cis-dihydroxy (C_2)	^1A 536 (53.3)	0.000	^1B 467 (61.3)	0.492	^1A 406 (70.5)	0.033	^1B 324 (88.3)	0.015	^1B 289 (98.9)	0.478
trans-dimethoxy (C_2)	^1A 585 (48.9)	0.000	^1A 479 (59.7)	0.006	^1B 472 (60.5)	0.033	^1B 321 (89.1)	0.107	^1B 271 (105.6)	0.275
cis-dimethoxy (C_2) (1)[a]	^1A 522 (54.8)	0.094	^1B 473 (60.4)	0.369	^1A 400 (71.5)	0.000	^1B 326 (87.5)	0.003	^1B 183 (156.4)	0.669
cis-dimethoxy (C_2) (2)[a]	^1A 459 (62.3)	0.000	^1B 448 (63.8)	0.488	^1A 418 (68.5)	0.035	^1B 322 (88.8)	0.001	^1B 276 (103.6)	0.449

[a]Two *cis*-dimethoxy isomers were determined to be close in energy on the ground state and so both are thought to play a role in the spectrum (see Ref. [125])

Table 4 SSA-MRMP2(8e,8o)/6-311G(d,p)//CIS/6-31G(d) emissions in nm and kcal/mol (in brackets)[a]

Compound	$S_2' \rightarrow S_0'$	OS	$S_3' \rightarrow S_0'$	OS
trans-dihydroxy (C_2)	^1B 7672 (3.7)	0.001	–	–
cis-dihydroxy (C_2)	^1B616 (46.5)	0.538	–	–
trans-dimethoxy (C_2)	–	–	^1B 666 (42.9)	0.237
cis-dimethoxy (C_2) (1)	^1B 612 (46.7)	0.462	–	–
cis-dimethoxy (C_2) (2)	^1B 584 (49.0)	0.532	–	–

[a]The origin of the emissive state as S_n' where $n > 1$ is not meant to suggest a violation of Kasha's rule, where fluorescence originates from the lowest lying excited singlet state. The calculated transition energies correspond to transition energies between the SSA-MRMP2/6-311G(d,p) *lowest energy* excited states and ground states at the CIS/6-31G(d) relaxed geometries; the *n* denotes the origin of the states at the SSA-MRMP2/6-311G(d,p)//RHF/6-31G(d) level of theory *before* CIS/6-31G(d) geometry relaxation (Table 3)

For the dihydroxy system, the calculated transition energies and OS indicate that the broad weak absorption between ~450–800 nm is due to $S_0 \rightarrow S_2$ and $S_0 \rightarrow S_3$ ^1B transitions, and the higher intensity higher energy peaks are due to $S_0 \rightarrow S_4$ and $S_0 \rightarrow S_5$ ^1B transitions. The ^1A transitions, while not symmetry forbidden, are predicted to be dark i.e. they have very small CASSCF oscillator strengths. CIS/6-31G(d) geometry optimization of the first excited ^1B state of the *trans*-dihydroxy isomer leads to a hydrogen transfer. The resulting C_2 structure, which is a minimum on the CIS S_1 surface, closely resembles the C_2 S_0 transition state discussed above (Fig. 6). This excited state geometry relaxation leads to an SSA-MRMP2 $S_2' \rightarrow S_0'$ ^1B transition that is predicted to be at a very long wavelength > 7000 nm (3.7 kcal/mol) (Table 4). This obviously does not correspond to the observed emission at ~350 nm (Fig. 4). We have previously speculated that this small energy gap, resulting from the close approach of the ^1A S_0 and ^1B S_2 surfaces, leads to large inter-electronic state vibronic coupling and consequently very rapid nonradiative decay to the ground state surface. We are unable to explicitly calculate the nonadiabatic coupling matrix elements to confirm this though. Figure 7 summarizes this absorption/nonradiative decay process in a schematic representation (not to scale). For the *cis*-dihydroxy isomer, where no such excited state hydrogen transfer can take place, the calculated $S_2' \rightarrow S_0'$ ^1B transition is 616 nm (Table 4), and has sizeable oscillator strength. This does not correspond to the observed emission in the experimental spectrum either, and we concluded that this is further evidence that the *cis* isomer is probably not present [125]. The calculated transition energies suggest, then, that the intense blue emission observed experimentally at ~350 nm is in fact due to a transition in the *trans* isomer from a state other than the lowest energy state S_2', possibly *trans* S_5'. We explained this clear violation of Kasha's rule,

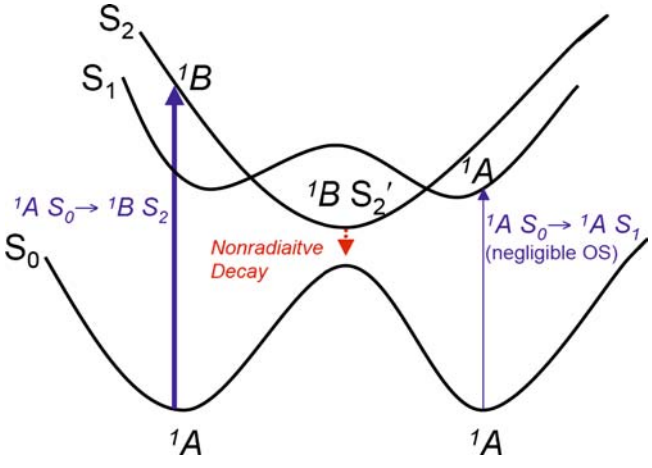

Fig. 7 Schematic representation (not to scale) of the suggested excited state processes (electronic states only) involving trans dihydroxy S_0, S_1, and S_2, based on computational results (Tables 3, 4 and Fig. 6) and the observed dihydroxy spectrum (Fig. 4). *Arrow thickness* is an indicator of OS or observed intensity. Note that only the S_0 minima and transition state, and S_2 minimum (S_2') have been determined and characterized computationally, as well as the vertical transitions shown. S_1 stationary points and the associated double-well S_1 surface are only suggested (i.e. have not been computationally determined), and nonradiative decay $S_2' \rightarrow S_0'$ is suggested based on the close approach of the two surfaces and corresponding likelihood of inter-electronic state vibronic coupling

which states that emission occurs from the lowest energy excited state, as a consequence of both a large energy gap between the upper and lower manifold of states (energy gap law) [134] and extremely rapid nonradiative decay from the lowest energy ^1B state to the ground state (see [125]).

For the *trans*- and *cis*-dimethoxy systems, calculated vertical transition energies and OS (see Table 3) suggest, simi-

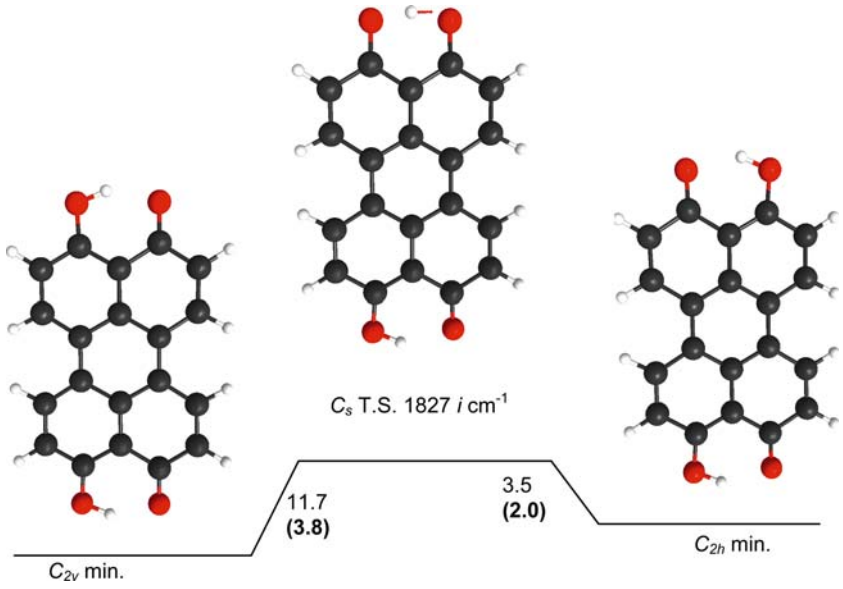

Fig. 8 Ground state hydrogen transfer in the hypocrellin model system (Fig. 2e, f). RHF/6-31G(d) energy barrier and MP2/6-31G(d)//RHF/6-31G(d) energy barrier (*bold* and in *brackets*) are given in kcal/mol (0 K and no ZPE). RHF/6-31G(d) imaginary frequency also given

larly to the dihydroxy case, that the broad weak absorptions in the visible region (∼450–650 nm) are due to $S_0 \rightarrow S_2$ and $S_0 \rightarrow S_3$ transitions [also $S_0 \rightarrow S_1$ for *cis*-dimethoxy(1)], while the more intense higher energy peaks are due to $S_0 \rightarrow S_4$ and $S_0 \rightarrow S_5$ transitions. The calculated $S_2' \rightarrow S_0'$ ($S_3' \rightarrow S_0'$ for the *trans* isomer) ^1B transition energies (Table 4) correspond well to the broad intense experimental emissions seen at ∼450–700 nm in the dimethoxy spectra. The fact that no hydrogen transfer can occur in these systems, and that emission in the visible is seen experimentally and is correctly predicted computationally, lends further weight to our findings for the dihydroxy case.

In summary, ab initio calculations along with experimental UV-visible spectra for the analog dihydroxy and dimethoxy perylene quinones, indicate that the dihydroxy molecule only exists in the *trans* form and undergoes rapid radiationless decay to the ground state from the lowest energy excited ^1B state. This, in turn, results in a lack of emission in the visible for the dihydroxy species.

3.2 4,9-dihydroxyperylene-3,10-quinone (model system)

Clearly the UV-visible spectrum of the dihydroxy analog compound (see Figs. 4, 2a) bears little resemblance to those of the naturally occurring perylene quinones (Figs. 1, 3), which do have emission spectra in the visible. This indicates that any excited state hydrogen transfer process in Hypocrellin A, for example, is quite different to that just seen, which results in nonradiative decay from the lower excited state to the ground state. The dihydroxy molecule 4,9-dihydroxyperylene-3,10-quinone (Fig. 2e, f), referred to as the *model system*, has its carbonyl and hydroxy groups in positions more closely resembling those in the natural products, especially Hypocrellin A (Fig. 1). Previous calculations, carried out by Chen et al. [135] at the CIS/6-31G level of theory only, suggest that for this model system the lowest state does not approach the ground state closely, but instead there are excited state surfaces well separated from the ground state, which control excited state transfer. If this were the case rapid radiationless decay would not occur and emission would be seen in the visible, more in line with the Hypocrellin A experimental spectrum. We now apply the same levels of theory to this model system as we did to the analog dihydroxy system to further examine the situation when dynamic electron correlation is accounted for.

Figure 8 depicts the ground state hydrogen transfer process in this model system. At the MP2/6-31G(d)//RHF/6-31G(d) level of theory, the lowest energy structure is the C_{2v} structure with both hydrogens on the same side. The barrier to a single hydrogen transfer to the C_{2h} structure is only 3.8 kcal/mol, and the C_{2h} isomer is only 1.8 kcal/mol higher in energy than the C_{2v} isomer (essentially degenerate). This suggests very rapid and continuous hydrogen transfer in the ground state. We note that no transition state exists on the classical PES for concerted double hydrogen transfer (direct C_{2v} to C_{2v}) in this system; the appropriate D_{2h} structure is high in energy and is also a higher order saddle point.

Tables 5 and 6 show calculated vertical absorption and emission energies, respectively. Again we see that CIS overestimates transition energies considerably compared to MRMP2. For this model system we have investigated the effects on calculated absorption energies (Table 5) of state averaging separately over only states of the same symmetry (SSA), including three states per symmetry, versus averaging over the first six states of any symmetry (SA), (state symmetry labels are still used for the latter as the symmetry character of the states are retained even though no symmetry is imposed).

Table 5 Calculated vertical absorption energies for the model dihydroxy system (Fig. 2e, f) in nm and kcal/mol (brackets). Oscillator strengths (OS), apart from the CIS case, are calculated at the corresponding CASSCF level of theory

	CIS/6-31G(d)[a]		SA-MRMP2 /6-31G(d)[b]		SA-MRMP2 /6-311G(d,p)[c]		SSA-MRMP2 /6-311G(d,p)[d]	
	Δ E	OS	Δ E	OS	Δ E	OS	Δ E	OS
C_{2v}								
$S_0 \rightarrow S_1$	$^1A_1$ 309 (92.5)	0.306	$^1A_1$ 499 (57.4)	0.261	$^1A_1$ 515 (55.6)	0.260	$^1A_1$ 533 (53.6)	0.260
$S_0 \rightarrow S_2$	$^1B_1$ 287 (99.7)	0.868	$^1B_1$ 364 (78.7)	0.033	$^1B_1$372 (76.9)	0.046	$^1B_1$390 (73.4)	0.046
$S_0 \rightarrow S_3$	$^1B_1$ 239 (119.6)	0.207	$^1B_1$ 354 (80.7)	0.592	$^1B_1$ 364 (78.6)	0.576	$^1B_1$ 383 (74.7)	0.576
$S_0 \rightarrow S_4$	$^1A_1$ 234 (122.0)	0.008	$^1A_1$ 353 (81.1)	0.007	$^1A_1$356 (80.4)	0.006	$^1B_1$339 (84.4)	0.370
$S_0 \rightarrow S_5$	$^1B_1$217 (131.5)	0.016	$^1B_1$318 (90.0)	0.416	$^1B_1$333 (86.0)	0.370	$^1A_1$248 (115.3)	0.006
C_{2h}								
$S_0 \rightarrow S_1$	^1B_u 347 (82.5)	0.518	^1A_g 638 (44.8)	0.000	^1B_u 531 (53.8)	0.376	^1B_u 534 (53.5)	0.376
$S_0 \rightarrow S_2$	^1B_u 283 (101.0)	0.575	^1B_u 513 (55.7)	0.384	^1B_u 440 (65.0)	0.334	^1A_g 496 (57.7)	0.000
$S_0 \rightarrow S_3$	^1A_g 248 (115.5)	0.000	^1B_u427 (67.0)	0.348	^1A_g 371 (77.1)	0.000	^1B_u 440 (65.0)	0.334
$S_0 \rightarrow S_4$	^1B_u 238 (119.9)	0.062	^1A_g 364 (78.5)	0.000	^1B_u 143 (199.7)	0.129	^1A_g 380 (75.3)	0.000
$S_0 \rightarrow S_5$	^1A_g 222 (128.7)	0.000	^1B_u 145 (196.9)	0.131	–	–	^1B_u 364 (78.7)	0.129

[a]CIS/6-31G(d)//RHF/6-31G(d)
[b]SA-MRMP2(8e,8o)/6-31G(d)//RHF/6-31G(d), averaged over six states
[c]SA-MRMP2(8e,8o)/6-311G(d,p)//RHF/6-31G(d), averaged over six states
[d]SSA-MRMP2(8e,8o)/6-311G(d,p)//RHF/6-31G(d), two separate calculations, one averaged over three symmetric states and one averaged over three asymmetric states

Table 6 Calculated vertical emission energies for the model dihydroxy system (Fig. 2e, f) in nm and kcal/mol (brackets)

	CIS/6-31G(d)[a]		SA-MRMP2/6-31G(d)[b]	
	Δ E	OS	Δ E	OS[c]
C_{2v}[e]				
$S_1' \rightarrow S_0'$	$^1A_1$ 369 (77.5)	0.330	$^1A_1$ 617 (46.3)	0.322
$S_2' \rightarrow S_0'$	$^1B_1$327 (87.4)	1.100	$^1B_1$413 (69.2)	0.721
$S_3' \rightarrow S_0'$	$^1B_1$ 282 (101.6)	0.017	$^1B_1$ 395 (72.3)	0.062
C_{2h}[e]				
$S_1' \rightarrow S_0'$	^1B_u 409 (70.0)	0.503	^1B_u 610 (46.9)	0.400
$S_2' \rightarrow S_0'$	^1B_u 311 (91.9)	0.677	^1B_u 442 (64.7)	0.431
$S_3' \rightarrow S_0'$	^1A_g 267 (107.0)	0.000	^1A_g 457 (62.6)	0.104[f]

[a]CIS/6-31G(d)//CIS/6-31G(d)
[b]SA-MRMP2(8e,8o)/6-31G(d)//CIS/6-31G(d), state averaged over six states
[c]OS calculated at the corresponding CASSCF level of theory
[e]No symmetry constraints were imposed during CIS geometry optimizations nor were the final structures symmetrized. Point groups and state symmetries are given as structures and states largely retain their symmetry character
[f]Non zero OS indicates state symmetry not preserved at CASSCF level of theory

We have also investigated basis set effects. These comparisons were carried out in part with future studies of Hypocrellin A in mind: Hypocrellin A has C_1 point group symmetry and due to its size it is useful to know how the smaller basis set performs. The CASSCF absorption transition energies are not presented here, but again overestimate transition energies compared to MRMP2. In addition, there is less than ∼1 kcal/mol difference in transition energies between the 6-31G(d) and 6-311G(d,p) basis sets for SA-CASSCF, and the SSA-CASSCF values generally differ with SA-CASSCF/6-311G(d,p) by less than ∼2 kcal/mol. For the C_{2v} isomer at the SA-MRMP2 levels of theory, only a small basis set effect is observed, with slightly smaller transition energies for the 6-311G(d,p) basis set (difference of ∼2 kcal/mol in most cases). Comparing the SA-MRMP2 level of theory with the SSA-MRMP2 level of theory (both 6-311G(d,p)), symmetry state averaging generally results in smaller transition energies (difference of ∼4 kcal/mol or less for the first $^1A_1$ excited state and all $^1B_1$ states), but there is a significant discrepancy for the higher $^1A_1$ state. The totally symmetric excited states appear in general to be particularly sensitive regarding the reference used for correlation treatment (see below also), and we plan to investigate the effects of larger active spaces on these correlated states. For the C_{2h} isomer, there is, with one exception, good agreement for the ^1B_u states between all MRMP2 levels of theory. The exception is the highest energy ^1B_u state, which has a significantly lower transition energy according to SSA-MRMP2 than according to SA-MRMP2 (196.9 and 199.7 vs. 78.7 kcal/mol, respectively). This may be simply due to the fact that in the case of SSA-MRMP2 only three states are averaged over at a time compared to six for SA-MRMP2, meaning there are fewer constraints in the SSA-MRMP2 calculation. For the ^1A_g states the situation is somewhat analogous: one of the ^1A_g state's transition energies is similar at all three levels of theory (78.5, 77.1, and 75.3 kcal/mol); the remaining ^1A_g state drops down to the

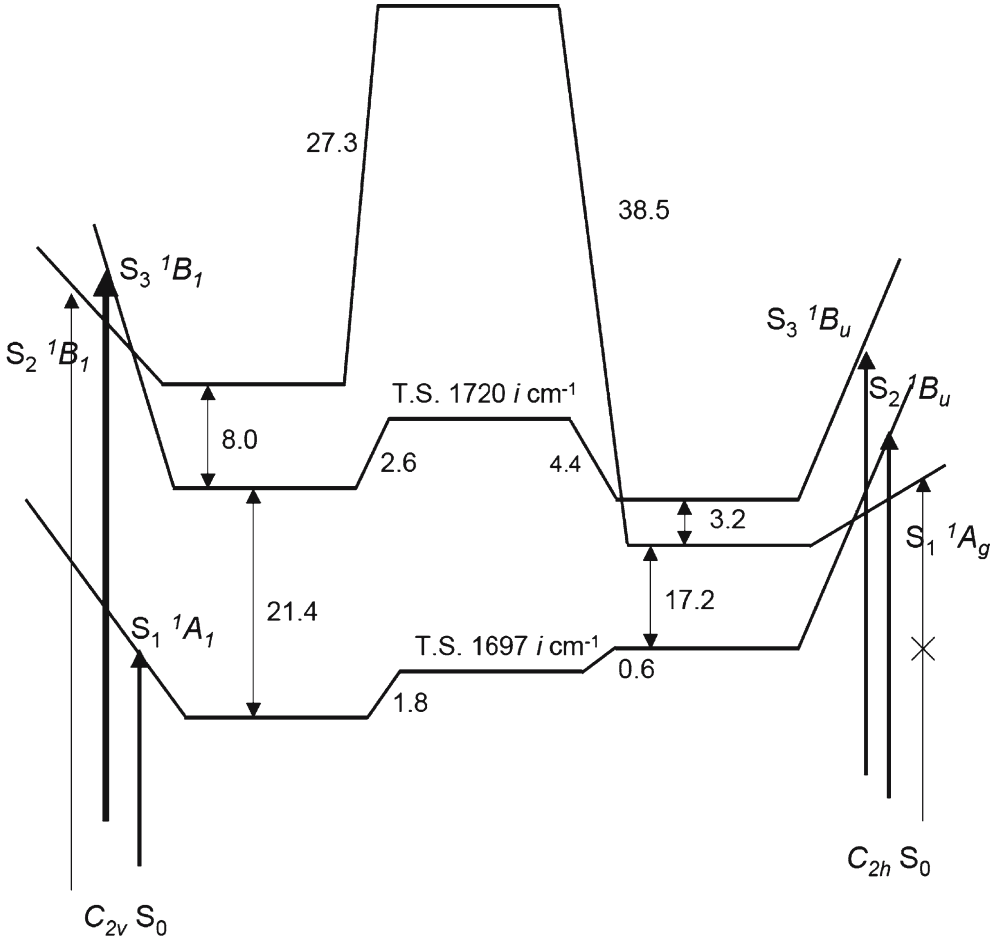

Fig. 9 Excited state relative energies at the SA-MRMP2(8e,8o)/6-31G(d)//CIS/6-31G(d) level of theory. Imaginary frequencies were calculated at the CIS/6-31G(d) level of theory. *Arrow thickness* is an indication of calculated oscillator strength (see Table 5)

S_1 state for SA-MRMP2/6-31G(d) and to the S_2 state at the SSA-MRMP2/6-311G(d,p) level, but is extremely high in energy at the SA-MRMP2/6-311G(d,p) level. We note that this particular state has a large double-excitation character. The reasons for the inconsistent results described are not presently clear. All the CASSCF active spaces are qualitatively the same and the CASSCF transition energies themselves agree very well, suggesting the references are consistent. As mentioned above we plan to investigate the effect of going to larger active spaces (also see future directions below). We do note, though, that most serious problems lie with the higher energy states and with the C_{2h} ^1A_g symmetry forbidden state, and so the current results still have utility. Table 6 shows the calculated emission transition energies. Even though the geometries are not strictly symmetric (C_1 geometry optimizations at the CIS/6-31G(d) level of theory), state symmetry labels are used as their symmetry character is largely retained.

It is interesting to compare the MRMP2 absorption and emission energies of this model system with the UV-visible spectrum of Hypocrellin A (Fig. 3). Consider the gross structure of the spectrum: a broad intense peak centered at ~475 nm, and two less intense peaks at ~550 and ~575 nm. Now comparing with the calculated lower energy transitions and OS for both C_{2v} and C_{2h} isomers, (first three states ($^1A_1$ and $^1B_1$) only for C_{2v} and first two ^1B_u states only for C_{2h}, meaning that the problem states described above are avoided), it can be seen that the gross features of the spectrum are reproduced albeit shifted to the blue. For example, SSA-MRMP2/6-311G(d,p), with OS inferred from SA-CASSCF, predicts a medium intense absorption, ^1B_u 534 nm, $^1A_1$ 533 nm, another medium intense absorption, ^1B_u 440 nm, and an intense absorption, $^1B_1$ 383 nm. This suggests that the perylene core with this arrangement of carbonyl and hydroxy groups does account for the gross features of the Hypocrellin A spectrum. The experimental emission spectrum (Fig. 3) has its most intense peak at ~625 nm; the SA-MRMP2/6-31G(d) $S_1' \rightarrow S_0'$ transitions in Table 6 are most relevant and are $^1A_1$ 617 and ^1B_u 610 nm.

Figure 9 shows the SA-MRMP2/6-31G(d) relative energies at the first three excited state CIS/6-31G(d) stationary points, i.e., SA-MRMP2/6-31G(d)//CIS/6-31G(d) at each state. (CIS/6-31G(d) imaginary frequencies are also presented for two of the states). This figure is intended only to summarize the calculated MRMP2 single point excited state *relative*

Table 7 Relative energies of four hypocrellin A (Fig. 1a, 10) hydrogen transfer tautomers in kcal/mol for the ground S_0 and first excited state S_1

	RHF/6-31G(d) S_0	MP2/6-31G(d)[a] S_0	CIS/6-31G(d) S_1
Normal Tautomer	0.0	0.0	0.0 [0.0][b]
T.S.(1)	11.3	3.0	5.9 [5.1][b]
Mono Tautomer (1)	3.6	0.1	−4.1 [−5.1][b]
T.S.(2)	11.1	1.6	7.4
Double Tautomer	0.3	−2.1	3.0
T.S.(3)	11.9	2.3	7.6
Mono Tautomer (2)	4.5	0.7	−3.8
T.S.(4)	11.6	3.1	5.8

[a]Single point energies: MP2/6-31G(d)//RHF/6-31G(d)
[b]Value in square brackets is for corresponding CIS/6-31G(d) S_1 relative energies for the model system (Fig. 2e, f)

energies, and any "surface crossings" in the figure arise as a result of states switching order at the SA-MRMP2 level on going from the ground state geometries to CIS/6-31G(d) excited state geometries. We also note that a CIS MEP, confirming minima correspond with transition states, was only determined for S_1. The basic finding is that on the surfaces labeled S_1 and S_3, the difference in energies between the hydrogen-transferred structures is small, and energy barriers, if any, are also small, leading to the conclusion that excited state hydrogen transfer is very likely.

In summary, calculations on the hypocrellin model system (Fig. 2e–f) predict very different behavior from the analog [125] system (Fig. 2a). In the model system, hydrogen transfer is predicted to occur easily in the excited state; however, the excited state surfaces do not approach the ground state surface (even at the correlated level of theory) and emission in the visible would be expected. The calculated absorption and emission energies for the model system appear to reproduce gross features of the hypocrellin A spectrum only slightly blue shifted. This suggests the gross features of the Hypocrellin A steady state spectrum are due to the perylene core plus positioning of the carbonyl and hydroxy groups. Some inconsistencies between MRMP2 levels of theory exist and larger active spaces need to be investigated.

3.3 Hypocrellin A

We now present some initial results for the hypocrellin A molecule itself (Fig. 1a). While isomers with a number of arrangements of the hypocrellin A seven-membered ring have been found experimentally [136], at this early stage we only consider one such isomer, and examine the ground and excited hydrogen transfer processes for it. Table 7 shows the ground state relative energies of four hydrogen transfer tautomers (see Fig. 10) of hypocrellin A and the transition states linking them. At the MP2/6-31G(d)//RHF/6-31G(d) level of theory all minima are within ∼3 kcal/mol of each other and the largest barrier is ∼4 kcal/mol. This suggests continuous hydrogen transfer in the ground state. Also, in Table 7 are CIS/6-31G(d) S_1 relative energies. At this level of theory minima differ by up to ∼7 kcal/mol with the mono tautomers lower in energy than the normal and double tautomer, while hydrogen transfer barriers are as high as ∼11 and as low as ∼6 kcal/mol. Based on the above findings for the model compound one might expect a reduction in these energy differences and transfer barriers with the inclusion of dynamic electron correlation. For example, for the model system at the CIS/6-31G(d) level of theory, S_1 relative energies for the hydrogen transfer process (C_{2v} to C_{2h}) are 0.0, 5.1, and−5.1 kcal/mol; at the SA-MRMP2 level they are 0.0, 1.8, and 2.4 kcal/mol (see Fig. 9). Note the similarity of the CIS/6-31G(d) relative energies for the normal tautomer, T.S.(1), and double tautomer, (0.0, 5.9, and −4.1 kcal/mol, respectively), with those of the model system.

Absorption and emission transition energies, and corresponding OS for all four hypocrellin A tautomers (Fig. 10) have been calculated at the CIS/6-31G(d) level of theory. Tables 8 and 9 present the results for just the normal tautomer and mono tautomer (1); for an interesting comparison Table 8 also presents absorption energies and OS for C_2 hypericin (from a previous study this is the lowest energy structure [137]) (Fig. 1b). Comparison of hypocrellin A results with the corresponding CIS data for the model system (Tables 5, 6) shows considerable similarities. First, the absorption OS follow almost the same patterns in terms of intensity, which match well with the experimental spectrum. In addition, the absorption transition energies, while a little smaller (i.e. red shifted), are quite similar to those for the model system for the first few states (e.g. for $S_0 \rightarrow S_1$ 90.8 compared to 92.5 kcal/mol, and for $S_0 \rightarrow S_2$ 95.2 compared to 99.7 kcal/mol, for normal hypocrellin A (Table 8) versus the C_{2v} model (Table 5), respectively. Some of the higher states have larger differences with a maximum difference ∼13 kcal/mol. It is reasonable to expect a similar sized dynamic electron correlation effect to that in the model system. Based on this, a simple scaling of the lower few states would result in a decent match up with the gross features of the hypocrellin A absorption spectrum. Interestingly, hypericin's CIS OS also follow the intensity pattern seen in its experimental spectrum (Fig. 3); again a simple scaling would be effective. Inspection of Table 9 and comparison with Table 6 shows similar to the absorption case that the CIS/6-31G(d) vertical emission transition energies for hypocrellin A are reduced slightly compared to the model system, again a simple scaling based on the model's correlation effect puts this emission in the correct region. We intend to explicitly in-

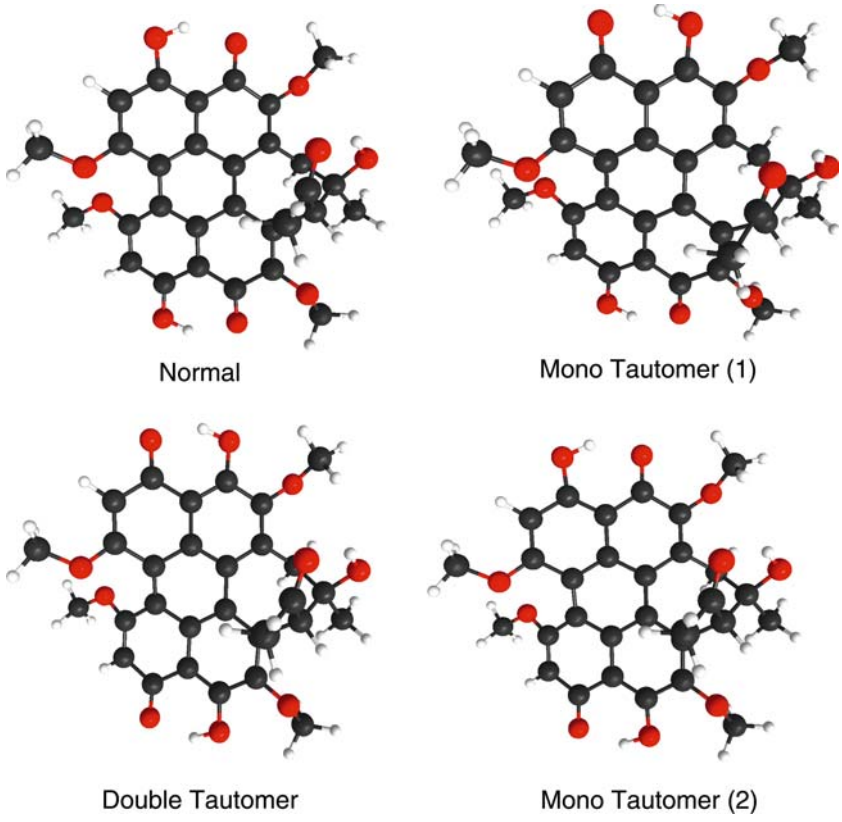

Fig. 10 The four ground state Hypocrellin A hydrogen transfer tautomers considered in this study

Table 8 CIS/6-31G(d)//RHF/6-31G(d) vertical absorption energies for the normal tautomer and mono tautomer (1) (Fig. 10) and C_2 hypericin (Fig. 1b) in nm and kcal/mol (brackets)

	$S_0 \rightarrow S_1$	OS	$S_0 \rightarrow S_2$	OS	$S_0 \rightarrow S_3$	OS	$S_0 \rightarrow S_4$	OS	$S_0 \rightarrow S_5$	OS
Normal	315 (90.8)	0.332	300 (95.2)	0.817	262 (109.1)	0.012	253 (113.2)	0.040	241 (118.7)	0.001
Mono(1)	354 (80.8)	0.513	296 (96.5)	0.457	265 (108.0)	0.036	256 (111.6)	0.128	234 (122.2)	0.001
Hypericin (C_2)	^1A 324 (88.2)	0.661	^1B 291 (98.3)	0.301	^1A 265 (108.0)	0.002	^1B 258 (110.9)	0.012	^1A 245 (116.5)	0.093

Table 9 CIS/6-31G(d)//CIS/6-31G(d) vertical emission energies for the normal tautomer and mono tautomer (1) (Fig. 10) in nm and kcal/mol (brackets)

	$S_1' \rightarrow S_0'$	OS
Normal	397 (72.1)	0.348
Mono(1)	435 (65.8)	0.503

clude dynamic correlation effects in future work on both the hypocrellin A and hypericin systems.

In summary, we have carried out initial calculations on the hypocrellin A system (143 occupied orbitals and 652 basis functions), and have shown that ground state hydrogen transfer is a low energy barrier process at the MP2 level of theory. Furthermore, from CIS/6-31G(d) calculations on hypocrellin A and by analogy with the model system in the previous section, we conclude excited state hydrogen transfer is a low energy process on the S_1 surface also. It is also quite clear that the S_1 hydrogen transfer surface for hypocrellin A will not approach the ground state surface, contrary to the situation for the dihydroxy analog [125], which is quite consistent with existence of an emission spectrum in the visible (Fig. 3).

4 Conclusions, future directions, and future prospects

It was determined, through ab initio electronic structure calculations and an adiabatic Frank-Condon approach, that the lack of emission in the visible in the experimental UV-visible spectrum of a dihydroxy perylene quinone molecule (Figs. 2a, 4), originally designed as a hypocrellin/hypericin analog [125], is probably due to the close approach of the ground and excited state hydrogen transfer surfaces, which in turn results in a rapid nonradiative decay to the ground state (Fig. 7). Next, upon the basis of calculations on a model system (Fig. 2e, f), bearing a closer resemblance to hypocrel-

lin, and initial calculations on the full hypocrellin A molecule itself (Fig. 1a), we concluded that the very different emission behavior by hypocrellin A (Fig. 3) compared to the dihydroxy analog (Fig. 4), is due to the fact that the hypocrellin A excited state hydrogen transfer surfaces are well separated from the ground state surface.

MRMP2 calculations on the model system (Fig. 2e, f) produced some inconsistent results, most notably for a totally symmetric state with large double-excitation character and some higher energy states. That the results for these cases were so sensitive to the reference orbitals, and how they were generated, highlights one of the difficulties of the CASSCF and MRMP2 approaches. We are about to initiate an examination of the effect of going to larger active spaces at the MRMP2 level for these cases. A parallelized fully direct determinant based MRMP2 algorithm recently designed and implemented by Joseph Ivanic (private communication), has only now made these larger active space calculations with the 6-311G(d,p) basis set feasible. Of course, the choice of active orbitals is vital, and although we are careful to examine our active spaces for consistency, it becomes harder with the increasing size of the system to be sure that the best possible active space for the excited states required has been found. We are currently implementing an automated scheme based on CIS state averaged natural orbitals, which we hope will generate unbiased active space starting orbitals for a given number of excited states.

In future work we will apply MRMP2 to the full Hypocrellin A molecule, again using a newly implemented fully direct MRMP2 parallel algorithm. We also plan to examine the performance of TDDFT for these hydrogen transfer systems, due to its potential for providing fairly accurate energetics for a similar cost to CIS. Other issues we hope to address are solvation and hydrogen tunneling effects. Examination of hypocrellin A's dependence on solvent viscosity [20, 21], will require an explicit solvent method and work has already begun on a CIS-EFP excited state solvation approach. As a ground state DFT-EFP has already been developed [138, 139], clearly a DFT/CIS-EFP or even TDDFT-EFP approach would be a natural extension, given the limitations of CIS. The effects of heavy atom motion (for example hypocrellin A's seven-membered ring motion [22, 23]) on hydrogen tunneling behavior (excited state and ground state) could, in the future, be examined by displacement along ground and excited state normal modes, and numerical calculation of the hydrogen wavefunction [115, 119] at points along this displacement. Reasonable energetics at a reasonable cost are essential for this approach underlining the need to benchmark the TDDFT and DFT/CIS methods for these systems. Another approach to the tunneling issue in the long term may be the NEO method [121, 122].

In conclusion, ab initio studies of excited state hydrogen transfer reactions in medium to large systems that allow, to a degree, interpretation of experimental data are starting to become possible. Future prospects for advancement in this area relies heavily on the availability of fast but accurate ab initio excited state potentials for medium to large systems, and this is clearly a highly active area of research. The further development of QM-MM approaches will presumably play an important role in examination of excited state solvation effects, and even excitations in biological systems, for example, prediction of absorption shifts on DNA-drug complexation. Ab initio computational studies of complex excited state phenomena such as conical intersections, vibronic coupling, hydrogen tunneling, and excited state dynamics for large systems will remain a huge challenge for sometime to come, mainly due to the cost of the excited state ab initio potential and its derivatives.

Acknowledgements Thanks to Dr. Jack Collins and Prof. Mark Gordon for their careful reading of the manuscript and useful suggestions. Thanks also to Prof. Jake Petrich for providing UV-visible spectra. All calculations were carried out using the computer facilities at the Advanced Biomedical Computing Center. This project has been funded in part with Federal funds from the National Cancer Institute, National Institutes of Health, under Contract No. N01-CO-12400. The content of this publication does not necessarily reflect the views or policies of the Department of Health and Human Services, nor does mention of trade names, commercial products, or organization imply endorsement by the US Government.

References

1. Hudson JB, Zhou J, Chen J, Harris L, Yip L, Towers GHN (1994) Photochem Photobiol 60: 253
2. Carpenter S, Fehr MJ, Kraus GA, Petrich JW (1994) Proc Natl Acad Sci USA 91:12273
3. Agostinis P, Vantieghem A, Merlevede W, de Witte PAM (2002) Int J Biochem. Cell Biol 34:221
4. Mirossay A, Mojzis J, Tothova J, Hajikova M, Lackova A, Mirossay L (2000) Phytomedicine 7:471
5. Kamuhabwa AAR, Roskams T, D'Hallewin MA, Baert L, Van Poppel H, De Witte PAM (2003) Int J Cancer 107:460
6. Dumas S, Lepretre JC, Lepellec A, Darmanyan A, Jardon P (2004) J Photochem Photobiol A Chem 163:297
7. Hadjur C, Jardon P (1995) J Photochem Photobiol B Biol 29:147
8. Chaloupka R, Sureau F, Kocisova E, Petrich JW (1998) Photochem Photobiol 68:44
9. Fehr MJ, McCloskey MA, Petrich JW (1995) J Am Chem Soc 117:1833
10. Wills NJ, Park J, Wen J, Kesavan S, Kraus GA, Petrich JW, Carpenter S (2001) Photochem Photobiol 74:216
11. Das K, Smirnov AV, Snyder MD, Petrich JW (1998) J Phys Chem B 102:6098
12. Petrich JW (2000) Int Rev Phys Chem 19:479
13. Chowdhury PK, Das K, Datta A, Liu WZ, Zhang HY, Petrich JW (2002) J Photochem Photobiol A Chem 154:107
14. Smirnov AV, Das K, English DS, Wan Z, Kraus GA, Petrich JW (1999) J Phys Chem A 103:7949
15. Yarkony DR (2001) J Phys Chem A 105:6277
16. Truhlar DG, Mead CA (2003) Phys Rev A 68:032501
17. Bernardi F, Olivucci M, Robb MA (1996) Chem Soc Rev 25:321
18. Lengsfield BH, Yarkony DR (1992) In: Baer M, Ng C-Y (eds) State-selected and state-to state ion-molecule reaction dynamics, Part 2: theory (Advances in chemical physics series), vol LXXXII. Wiley, New York, p 1
19. Gai F, Fehr MJ, Petrich JW (1994) J Phys Chem 98:8352
20. Das K, English DS, Fehr MJ, Smirnov AV, Petrich JW (1996) J Phys Chem 100:18275
21. Das K, English DS, Petrich JW (1997) J Am Chem Soc 119:2763
22. Das K, English DS, Petrich JW (1997) J Phys Chem A 101:3241
23. Das K, Dertz E, Paterson J, Zhang W, Kraus GA, Petrich JW (1998) J Phys Chem B 102:1479

24. Foresman JB, Head-Gordon M, Pople JA, Frisch MJ (1992) J Phys Chem 96:135
25. Shroll RM, Edwards WD (1997) Int J Quantum Chem 63:1037
26. Maurice D, Head-Gordon M (1999) Mol Phys 96:1533
27. An example is the parallel AO based, fully direct, CIS frozen core energy and gradient code devloped at the Advanced Biomedical Computing Center (ABCC) by S. P. Webb and implemented in the electronic structure package GAMESS
28. Head-Gordon M, Maurice D, Oumi M (1995) Chem Phys Lett 246:114
29. Grimme S, Ugorodina EI (2004) Chem Phys 305:223
30. Maurice D, Head-Gordon M (1995) Int J Quantum Chem 29:361–370
31. Maurice D, Head-Gordon M (1996) J Phys Chem 100:6131
32. Grimme S (1996) Chem Phys Lett 259:128
33. Head-Gordon M, Grana AM, Maurice D, White CA (1995) J Phys Chem 99:14261
34. Schmidt MW, Gordon MS (1998) Annu Rev Phys Chem 49:233
35. Roos BO, Taylor PR (1980) Chem Phys 48:157
36. Ruedenberg K, Cheung LM, Elbert ST (1979) Int J Quantum Chem 16:1069
37. Webb SP, Gordon MS (1998) J Chem Phys 109:919
38. Webb SP, Gordon MS (1998) J Am Chem Soc 120:3846
39. Pipek J, Mezey PG (1989) J Chem Phys 90:4916
40. Bauschlicher CW (1980) J Chem Phys 72:880
41. Sherrill CD, Schaefer HF (1999) Adv Quantum Chem 34:143
42. Gan ZT, Alexeev Y, Gordon MS, Kendall RA (2003) J Chem Phys 119:47
43. Klene M, Robb MA, Frisch MJ, Celani P (2000) J Chem Phys 113:5653
44. Boggio-Pasqua M, Bearpark MJ, Klene M, Robb MA (2004) J Chem Phys 120:7849
45. Olsen J, Roos BO, Jorgensen P, Jensen HJA (1988) J Chem Phys 89:2185
46. Malmqvist PA, Rendell A, Roos BO (1990) J Phys Chem 94:5477
47. Klene M, Robb MA, Blancafort L, Frisch MJ (2003) J Chem Phys 119:713
48. Ivanic J (2003) J Chem Phys 119:9364
49. Ivanic J (2003) J Chem Phys 119:9377
50. Panin AI, Simon KV (1996) Int J Quantum Chem 59:471
51. Andersson K, Malmqvist PA, Roos BO, Sadlej AJ, Wolinski K (1990) J Phys Chem 94:5483
52. Andersson K, Malmqvist PA, Roos BO (1992) J Chem Phys 96:1218
53. Hirao K (1992) Chem Phys Lett 196:397
54. Hirao K (1993) Chem Phys Lett 201:59
55. Nakano H (1993) J Chem Phys 99:7983
56. Nakano H (1993) Chem Phys Lett 207:372
57. Khait YG, Song J, Hoffmann MR (2002) J Chem Phys 117:4133
58. Roos BO (1999) Acc Chem Res 32:137
59. Roos BO, Andersson K, Fulscher MP, Malmqvist PA, SerranoAndres L, Pierloot K, Merchan M (1996) Adv Chem Phys 93:219
60. Gross EUK, Dobson JF, Petersilka M (1996) In: Nalewajski RF (ed) Density functional theory II. Springer, Berlin Heidelberg New York
61. Casida ME (1995) In: Chong DP (ed) Recent advances in density functional methods, vol 1. World Scientific, Singapore
62. Parac M, Grimme S (2003) Chem Phys 292:11
63. Grimme S, Parac M (2003) Chem phys chem 4:292
64. Dreuw A, Weisman JL, Head-Gordon M (2003) J Chem Phys 119:2943
65. Neugebauer J, Baerends EJ, Nooijen M (2004) J Chem Phys 121:6155
66. Parac M, Grimme S (2002) J Phys Chem A 106:6844
67. Parusel ABJ, Grimme S (2001) J Porphyrins Phthalocyanines 5:225
68. Grimme S, Waletzke M (1999) J Chem Phys 111:5645
69. Khait YG, Hoffmann MR (2004) J Chem Phys 120:5005
70. Van Gisbergen SJA, Guerra CF, Baerends EJ (2000) J Comput Chem 21: 1511
71. Van Caillie C, Amos RD (2000) Chem Phys Lett 317:159
72. Van Caillie C, Amos RD (1999) Chem Phys Lett 308:249
73. Furche F, Ahlrichs R (2002) J Chem Phys 117:7433
74. Rappoport D, Furche F (2005) J Chem Phys 122(6):64105
75. Santos L, Vargas A, Moreno M, Manzano BR, Lluch JM, Douhal A (2004) J Phys Chem A 108:9331
76. Wanko M, Garavelli M, Bernardi F, Niehaus TA, Frauenheim T, Elstner M (2004) J Chem Phys 120:1674
77. Kowalski K, Piecuch P (2004) Mol Phys 102:2425
78. Musial M, Bartlett RJ (2004) J Chem Phys 121:1670
79. Tobita M, Perera SA, Musial M, Bartlett RJ, Nooijen M, Lee JS (2003) J Chem Phys 119:10713
80. Stanton JF, Bartlett RJ (1993) J Chem Phys 98:7029
81. Piecuch P, Kowalski K, Pimienta ISO, Fan PD, Lodriguito M, McGuire MJ, Kucharski SA, Kus T, Musial M (2004) Theor Chem Acc 112:349
82. Kowalski K, Piecuch P (2004) J Chem Phys 120:1715
83. Kucharski SA, Wloch M, Musial M, Bartlett RJ (2001) J Chem Phys 115: 8263
84. Nooijen M, Bartlett RJ (1997) J Chem Phys 106:6441
85. Nooijen M, Bartlett RJ (1997) J Chem Phys 107:6812
86. Nooijen M, Lotrich V (2000) J Chem Phys 113:494
87. Korona T, Werner HJ (2003) J Chem Phys 118:3006
88. Cramer CJ, Truhlar DG (1999) Chem Rev 99:2161
89. Tomasi J (2004) Theor Chem Acc 112:184
90. Gao J (1995) In: Lipkowitz KB, Boyd DB (eds) Reviews in computational chemistry, vol 7. VCH, New York, p 119
91. Day PN, Jensen JH, Gordon MS, Webb SP, Stevens WJ, Krauss M, Garmer D, Basch H, Cohen D (1996) J Chem Phys 105:1968
92. Gordon MS, Freitag MA, Bandyopadhyay P, Jensen JH, Kairys V, Stevens WJ (2001) J Phys Chem A 105:293
93. Webb SP, Gordon MS (1999) J Phys Chem A 103:1265
94. Merrill GN, Webb SP (2003) J Phys Chem A 107:7852
95. Merrill GN, Webb SP, Bivin DB (2003) J Phys Chem A 107:386
96. Merrill GN, Webb SP (2004) J Phys Chem A 108:833
97. Song J, Gordon MS, Deakyne CA, Zheng WC (2004) J Phys Chem A 108:11419
98. Damrauer R (2000) J Am Chem Soc 122:6739
99. Dobrogorskaia-Mereau, II, Nemukhin AV (2005) J Comput Chem 26:865
100. Karelson MM, Zerner MC (1992) J Phys Chem 96:6949
101. Cammi R, Mennucci B, Tomasi J (2000) J Phys Chem A 104:5631
102. Mennucci B, Cammi R, Tomasi J (1998) J Chem Phys 109:2798
103. Cossi M, Barone V (2001) J Chem Phys 115:4708
104. Krauss M, Webb SP (1997) J Chem Phys 107:5771
105. Jensen L, van Duijnen PT, Snijders JG (2003) J Chem Phys 119:3800
106. Dallos M, Lischka H, Shepard R, Yarkony DR, Szalay PG (2004) J Chem Phys 120:7330
107. Hazra A, Chang HH, Nooijen M (2004) J Chem Phys 121:2125
108. Nooijen M (2003) Int J Quantum Chem 95:768
109. Borgis D, Hynes JT (1996) J Phys Chem 100:1118
110. Alhambra C, Sanchez ML, Corchado J, Gao JL, Truhlar DG (2001) Chem Phys Lett 347:512
111. Albu TV, Corchado JC, Truhlar DG (2001) J Phys Chem A 105:8465
112. Hammes-Schiffer S (1998) J Phys Chem A 102:10443
113. Billeter SR, Webb SP, Iordanov T, Agarwal PK, Hammes-Schiffer S (2001) J Chem Phys 114:6925
114. Billeter SR, Webb SP, Agarwal PK, Iordanov T, Hammes-Schiffer S (2001) J Am Chem Soc 123:11262
115. Webb SP, Hammes-Schiffer S (2000) J Chem Phys 113:5214
116. Iordanov T, Billeter SR, Webb SP, Hammes-Schiffer S (2001) Chem Phys Lett 338:389
117. Ben-Nun M, Quenneville J, Martinez TJ (2000) J Phys Chem A 104:5161
118. Ben-Nun M, Martinez TJ (2000) J Chem Phys 112:6113
119. Webb SP, Agarwal PK, Hammes-Schiffer S (2000) J Phys Chem B 104:8884
120. Guallar V, Batista VS, Miller WH (2000) J Chem Phys 113:9510
121. Webb SP, Iordanov T, Hammes-Schiffer S (2002) J Chem Phys 117:4106

122. Pak MV, Swalina C, Webb SP, Hammes-Schiffer S (2004) Chem Phys 304: 227
123. Pak MV, Hammes-Schiffer S (2004) Phys Rev Lett 92:103002
124. Swalina C, Pak MV, Hammes-Schiffer S (2005) J Chem Phys 123:014303
125. Krishnamoorthy G, Webb SP, Nguyen PK, Chowdhury PK, Halder M, Wills NJ, Carpenter S, Kraus GA, Gordon MS, Petrich JW (2005) Photochem Photobiol 81:924
126. Gonzalez C, Schlegel HB (1989) J Chem Phys 90:2154
127. Harihara Pc, Pople JA (1973) Theor Chim Acta 28:213
128. Ditchfie R, Hehre WJ, Pople JA (1971) J Chem Phys 54:724
129. Hehre WJ, Ditchfie R, Pople JA (1972) J Chem Phys 56:2257
130. Fletcher GD, Rendell AP, Sherwood P (1997) Mol Phys 91:431
131. Krishnan R, Binkley JS, Seeger R, Pople JA (1980) J Chem Phys 72:650
132. Schmidt MW, Baldridge KK, Boatz JA, Elbert ST, Gordon MS, Jensen JH, Koseki S, Matsunaga N, Nguyen KA, Su SJ, Windus TL, Dupuis M, Montgomery JA (1993) J Comput Chem 14:1347
133. Dunning TH (1989) J Chem Phys 90:1007
134. Englman R, Jortner J (1970) Mol Phys 18:145
135. Chen DZ, Wang DP, Zhang HY, Tang B (2002) Chem Phys Lett 353:119
136. Smirnov A, Fulton DB, Andreotti A, Petrich JW (1999) J Am Chem Soc 121:7979
137. Petrich JW, Gordon MS, Cagle M (1998) J Phys Chem A 102:1647
138. Adamovic I, Freitag MA, Gordon MS (2003) J Chem Phys 118:6725
139. Adamovic I, Gordon MS (2005) J Phys Chem A 109:1629